OPTIMIZED MIMO SYMBOL MAPPING TO IMPROVE THE TURBO CLIFF REGION OF ITERATIVE PRECODED MIMO DETECTION

Nhat-Quang NHAN[*†], *Philippe ROSTAING*[*], *Karine AMIS*[†], *Ludovic COLLIN*[*], *Emanuel RADOI*[*]

[*] Université Européenne de Bretagne, France; Université de Brest ; CNRS, UMR 6285 LabSTICC
Email: {nhat-quang.nhan, philippe.rostaing, ludovic.collin, emanuel.radoi}@univ-brest.fr
[†] Télécom Bretagne, France; CNRS, UMR 6285 LabSTICC
Email: karine.amis@telecom-bretagne.eu

ABSTRACT

In this paper we investigate the concatenation of the multiple input multiple output (MIMO) $\max-d_{\min}$ linear precoder with an outer forward error correction (FEC) code assuming turbo detection at the receiver. A maximum squared Euclidean weight (MSEW) binary-to-MIMO symbol mapper is introduced in the precoding scheme. Extrinsic information transfer (EXIT) chart is used to analyze the turbo-cliff and error-floor of the proposed MIMO symbol mapper. Analysis and simulation results show significant improvement of the proposed MSEW symbol mapper in terms of error-rate performance.

Index Terms— MIMO linear precoder, turbo detection, iterative receiver, symbol mapping, EXIT chart.

1. INTRODUCTION

MIMO technology has become essential to take up the challenges of higher data rate and increasing data traffic that radio-cellular networks have to face up. It is one of the most crucial distinction between 3G and 4G wireless systems [1]. The idea of using multiple transceiver antennas not only offers the multiplexing and diversity gains, but it also achieves higher conventional point-to-point link reliability in comparison with single transmitter and single receiver systems [2]. The main challenge is to design a MIMO scheme that fully exploits the presence of multiple antennas. In time domain duplex (TDD) closed-loop schemes, the channel state information (CSI) is readily available at the transmitter through a feedback link, which enables to adapt the transmitter to the channel conditions. Several kinds of linear precoder have been proposed in the literature, differing from the design criteria among which the maximum minimum Euclidean distance in the received constellation (referred to as $\max-d_{\min}$ [3]), the minimum bit-error rate (BER) [4] or the maximum mutual information [5].

Most precoders have been designed without taking into account the outer FEC code. In this paper, we consider the concatenation of the $\max-d_{\min}$ precoder with a binary convolutional code. The turbo detection, introduced in [6] and later applied in many MIMO systems [7], is applied at the receiver. In most MIMO coded schemes, a binary to M-ary symbol conversion is inserted between the FEC code and the MIMO precoder. In this paper, we propose to directly address FEC-encoded symbols to the MIMO symbol mapper input. We assume perfect CSI at both the transmitter and the receiver. Our main contributions are threefold. First, we introduce a novel study case that takes into account the concatenation of the MIMO precoder with an outer FEC code assuming an iterative receiver. Second, we prove that the MIMO symbol mapping of the received constellation plays an essential role in error-rate performance of the turbo detection. Third, we demonstrate that the MSEW mapping is well adapted to use with $\max-d_{\min}$ precoder. In accordance to EXIT chart analyses, simulation results show that the improvement in terms of error-rate of the system is significant.

The remainder of this paper is organized as follows. Section 2 briefly introduces the system model along with the $\max-d_{\min}$ precoder and the soft demapper. Section 3 defines the MSEW MIMO symbol mapper and compares different mapping strategies. In Section 4, the essential role of the symbol mapper at the turbo-cliff and error-floor is discussed from EXIT charts. Simulated error rates are presented in Section 5 to validate the theoretical analysis. Section 6 concludes the paper and gives some perspectives.

2. SYSTEM MODEL AND PRELIMINARIES

2.1. System model

Let us consider a MIMO system with n_R receive, n_T transmit antennas and b independent data streams to be transmitted. We assume full-CSI at both the transmitter and the receiver. Information data bits are encoded by a binary recursive-systematic convolutional (RSC) code. The FEC codeword is then interleaved before entering the MIMO symbol mapper. In the MIMO symbol mapper, interleaved FEC-encoded bits are grouped into packets and each packet is mapped onto a b-dimensional symbol vector **s**. The vector **s** is then precoded
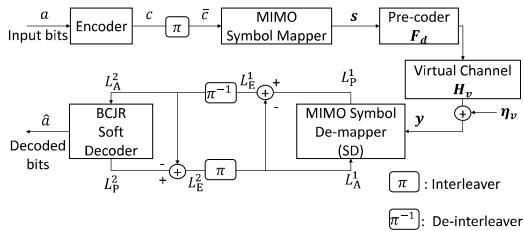
Fig. 1: Equivalent system model.

with $\mathbf{F}$ and transmitted through the MIMO channel. At the receiver side, after MIMO detection, a soft symbol demapper iteratively exchanges *extrinsic* information with a BCJR soft decoder [8]. The detection output, denoted by $\mathbf{y}$, reads

$$\mathbf{y} = \mathbf{GHFs} + \mathbf{G}\boldsymbol{\eta}, \tag{1}$$

where $\mathbf{F}$ is the $n_T \times b$ precoding matrix with the power constraint $\|\mathbf{F}\|_F^2 = 1$, $\|.\|_F$ is the Frobenius norm, $\mathbf{G}$ is the $b \times n_R$ detection matrix, $\mathbf{H}$ is the $n_R \times n_T$ channel matrix, and $\boldsymbol{\eta}$ is the $n_R \times 1$ additive white circularly-symmetric complex gaussian noise vector. Let $E[.]$ and $(.)^H$ stand for the expectation and the conjugate transpose respectively and let $\mathbf{I}_{n_R}$ be the identity matrix of size n_R. Then we assume $E[\boldsymbol{\eta}\boldsymbol{\eta}^H] = \sigma_\eta^2 \mathbf{I}_{n_R}$ and $E[\mathbf{ss}^H] = \sigma_s^2 \mathbf{I}_b$.

In this paper, we apply the same channel transformation as in [3]. Let us define $\mathbf{F}_d$ and $\mathbf{F}_v$ such that $\mathbf{F} = \mathbf{F}_v \times \mathbf{F}_d$. Matrices $\mathbf{F}_v$ and $\mathbf{G}$ are chosen so as to transform the MIMO channel into a virtual channel with b independent parallel sub-channels *i.e.*, the MIMO transmission becomes equivalent to b parallel transmissions of b independent streams. $\mathbf{F}_d$ denotes the new precoding matrix. It satisfies the power constraint $\|\mathbf{F}_d\|_F^2 = 1$. The equivalent writing of (1) is

$$\mathbf{y} = \mathbf{H}_v \mathbf{F}_d \mathbf{s} + \boldsymbol{\eta}_v, \tag{2}$$

where $\boldsymbol{\eta}_v$ is the $b \times 1$ virtual noise vector with $E[\boldsymbol{\eta}_v \boldsymbol{\eta}_v^H] = \sigma_\eta^2 \mathbf{I}_b$. The matrix $\mathbf{H}_v = \text{diag}(\sigma_1, ..., \sigma_b)$ is the $b \times b$ eigen-channel matrix, where $\{\sigma_1, ..., \sigma_b\}$ are the b most significant singular values of $\mathbf{H}$ sorted in descending order.

The equivalent system scheme is shown in Fig. 1, where L_A^1, L_P^1 and L_E^1 respectively stand for the *a priori*, the *a posteriori* and the *extrinsic* log likelihood ratios (LLRs) of the soft demapper, while those values for the BCJR soft decoder are L_A^2, L_P^2 and L_E^2.

2.2. The $\max{-}d_{\mathbf{min}}$ linear precoder

In this paper, we consider only quaternary quadrature amplitude modulation (4-QAM). We focus on a commonly used precoder named $\max{-}d_{\min}$ [3], in which $\mathbf{F}_d$ was designed to maximize the minimum Euclidean distance, denoted by $d_{min} = \min_{k \neq \ell} \|\mathbf{x}_k - \mathbf{x}_\ell\|$ where $\mathbf{x} = \mathbf{H}_v \mathbf{F}_d \mathbf{s}$, between the received constellation symbols. We restrict ourselves to $b = 2$. The conversion from cartesian to polar form of $\mathbf{H}_v$ gives

$$\mathbf{H}_v = \begin{pmatrix} \sigma_1 & 0 \\ 0 & \sigma_2 \end{pmatrix} = \rho \begin{pmatrix} \cos\gamma & 0 \\ 0 & \sin\gamma \end{pmatrix}, \tag{3}$$

where ρ and γ respectively represent the channel gain and angle. As $\sigma_1 \geq \sigma_2 > 0$, $0 < \gamma \leq \pi/4$. Hence, the optimal solution depends on γ and by defining the threshold $\gamma_0 = \arctan\sqrt{\frac{3\sqrt{3}-2\sqrt{6}+2\sqrt{2}-3}{3\sqrt{3}-2\sqrt{6}+1}}$ ($\approx 17,28^0$), $\mathbf{F}_d$ reads

- if $0 \leq \gamma \leq \gamma_0$

$$\mathbf{F}_d = \mathbf{F}_{r_1} = \begin{pmatrix} \sqrt{\frac{3+\sqrt{3}}{6}} & \sqrt{\frac{3-\sqrt{3}}{6}}e^{i\frac{\pi}{12}} \\ 0 & 0 \end{pmatrix}, \tag{4}$$

- if $\gamma_0 \leq \gamma \leq \pi/4$

$$\mathbf{F}_d = \mathbf{F}_{octa} = \frac{1}{\sqrt{2}} \begin{pmatrix} \cos\psi & 0 \\ 0 & \sin\psi \end{pmatrix} \begin{pmatrix} 1 & e^{i\frac{\pi}{4}} \\ -1 & e^{i\frac{\pi}{4}} \end{pmatrix}, \tag{5}$$

where $\psi = \arctan\frac{\sqrt{2}-1}{\tan\gamma}$. Note that ψ and γ_0 are SNR-independent.

2.3. MIMO Symbol Demapper (SD)

Let $\mathcal{Q}^b$ be the set of symbol vectors with the mapping rule defined by

$$\left(\alpha_1^k, ..., \alpha_q^k\right)_{\alpha_\ell^k \in \{0,1\}} \to \mathbf{s}_k \in \mathcal{Q}^b,$$

where $q = \log_2(Q)$, Q is the constellation size of $\mathcal{Q}^b$. The conditional probability density function (pdf) of the received vector $\mathbf{y}$ is defined by

$$p(\mathbf{y}|\mathbf{s} = \mathbf{s}_k) = \frac{1}{(\pi\sigma_\eta^2)^b} \exp\left(-\frac{\|\mathbf{y}-\mathbf{H}_v\mathbf{F}_d\mathbf{s}_k\|^2}{\sigma_\eta^2}\right). \tag{6}$$

Given $\mathbf{y}$, the *a posteriori* LLR of the bit at position i is calculated by

$$L_{P,i}^1 = \ln\frac{P(\alpha_i=1|\mathbf{y})}{P(\alpha_i=0|\mathbf{y})}. \tag{7}$$

Applying (6) with the Bayesian rule, we obtain

$$L_{P,i}^1 = \ln\frac{\sum_{\mathbf{s}_k \in \mathcal{Q}^b|\alpha_i=1} \exp\left(-\frac{\|\mathbf{y}-\mathbf{H}_v\mathbf{F}_d\mathbf{s}_k\|^2}{\sigma_\eta^2}\right)P(\mathbf{s}=\mathbf{s}_k)}{\sum_{\mathbf{s}_k \in \mathcal{Q}^b|\alpha_i=0} \exp\left(-\frac{\|\mathbf{y}-\mathbf{H}_v\mathbf{F}_d\mathbf{s}_k\|^2}{\sigma_\eta^2}\right)P(\mathbf{s}=\mathbf{s}_k)}. \tag{8}$$

At first iteration, the *a priori* probability is $P(\mathbf{s} = \mathbf{s}_k) = \frac{1}{Q}$ (equiprobability). From the second iteration, it is computed from L_E^2 by

$$P(\mathbf{s} = \mathbf{s}_k|L_E^2) = \prod_1^q P(\alpha_i = \alpha_i^k|L_E^2). \tag{9}$$

3. MIMO SYMBOL MAPPER

From (3), (4) and (5) it comes that $\mathbf{H}_v\mathbf{F}_d = a\mathbf{A}$, where $\mathbf{A}$ is a fixed matrix and a is a scalar, which depends on γ and ρ. Therefore, given $\mathbf{F}_d = \mathbf{F}_{r_1}$, the received constellation is unchanged and just scaled by a scalar factor a for each channel. The same holds for $\mathbf{F}_d = \mathbf{F}_{octa}$. With the chain rule of mutual information (MI), the bitwise MI of each bit of the received constellation symbols, which depends on the mapping rule of the symbol mapper, can be exploited to improve the performance of the turbo detection [9]. Let us remind that we focus on 4-QAM. Traditionally, every two bits of the codeword $\mathbf{c}$ are grouped and Gray-mapped into a 4-QAM symbol. Then, every $b = 2$ resulting 4-QAM symbol is converted from
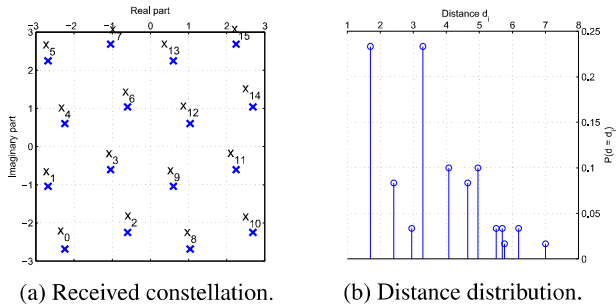
(a) Received constellation. (b) Distance distribution.

Fig. 2: Received constellation $\mathbf{x}_i$ and its Euclidean distance distribution in case $\mathbf{F}_d = \mathbf{F}_{r_1}$.

(a) First subchannel. (b) Second subchannel.

Fig. 3: Received constellation $\mathbf{x}_i$ on the first and second subchannel in case $\mathbf{F}_d = \mathbf{F}_{octa}$.

serial to parallel into the symbol vector $\mathbf{s}$. We refer the received constellation associated to this scheme as Gray-direct mapping.

In this study, we denote the 16 possible values of $\mathbf{s}$ by $\mathbf{s}_0 = [s_0 \, s_0]^T$, $\mathbf{s}_1 = [s_0 \, s_1]^T$, $\mathbf{s}_2 = [s_0 \, s_2]^T$, $\mathbf{s}_3 = [s_0 \, s_3]^T$, $\mathbf{s}_4 = [s_1 \, s_0]^T$, $\mathbf{s}_5 = [s_1 \, s_1]^T$, $\mathbf{s}_6 = [s_1 \, s_2]^T$, $\mathbf{s}_7 = [s_1 \, s_3]^T$, $\mathbf{s}_8 = [s_2 \, s_0]^T$, $\mathbf{s}_9 = [s_2 \, s_1]^T$, $\mathbf{s}_{10} = [s_2 \, s_2]^T$, $\mathbf{s}_{11} = [s_2 \, s_3]^T$, $\mathbf{s}_{12} = [s_3 \, s_0]^T$, $\mathbf{s}_{13} = [s_3 \, s_1]^T$, $\mathbf{s}_{14} = [s_3 \, s_2]^T$ and $\mathbf{s}_{15} = [s_3 \, s_3]^T$, where $s_0 = (-1-i)/\sqrt{2}$, $s_1 = (-1+i)/\sqrt{2}$, $s_2 = (1-i)/\sqrt{2}$, $s_3 = (1+i)/\sqrt{2}$ and $[.]^T$ stands for vector transposition. The encoded bits of $\mathbf{c}$ are grouped into length-4 packets and mapped directly onto $\mathbf{s}_i$ or equivalently mapped onto $\mathbf{x}_i = \mathbf{H}_v \mathbf{F}_d \mathbf{s}_i$, which defines the received constellation.

Three mapping techniques are considered in this paper: Gray-like, anti-Gray and MSEW. Let $\bar{\mathbf{s}}$ stands for the binary sequence mapped to $\mathbf{s}$. We define $\bar{d}_H(d_{min})$ the average Hamming distance $d_H(\bar{\mathbf{s}}_k, \bar{\mathbf{s}}_\ell)$ such that $d_{min} = \|\mathbf{x}_k - \mathbf{x}_\ell\|$. The Gray-like mapping aims to find the constellation such that $\bar{d}_H(d_{min})$ is minimized. Contrarily, the anti-Gray tries to maximize $\bar{d}_H(d_{min})$. Pioneered in [10], the purpose of MSEW is to minimize the error-floor of the single-input single-output (SISO) system used with the standard constellations and iterative receiver. We apply MSEW to MIMO $\max-d_{min}$ precoded system by using the two following mapping criteria. Firstly, we maximize the minimum Euclidean distance between symbols with binary mapped sequences differing by one position $d_{\mathrm{H}} = d_H(\bar{\mathbf{s}}_k, \bar{\mathbf{s}}_\ell) = 1$. This distance is denoted by l_1 in the remainder of the paper. This criterion is easy to apply to the received constellation of $\max-d_{min}$, since it was designed so as to maximize the minimum Euclidean distance between the constellation points. Secondly, we minimize the number of pairs of symbols with binary mapped sequences differing by one position ($d_{\mathrm{H}} = 1$) separated by the minimum Euclidean distance l_1.

Fig. 2a shows the received constellation on the first subchannel in the case $\mathbf{F}_d = \mathbf{F}_{r_1}$ ($\mathbf{F}_{r_1}$ spreads the power only on the first sub-channel). In case $\mathbf{F}_d = \mathbf{F}_{octa}$, the received constellations on the two sub-channels are shown in Fig. 3 ($\mathbf{F}_{octa}$ spreads power in both sub-channels).

Table 1 provides optimized mappings (but not unique) for each mapping strategy applied to the received constellation for $\mathbf{F}_{r_1}$ in Fig. 2 and for $\mathbf{F}_{octa}$ in Fig. 3. Note that we have
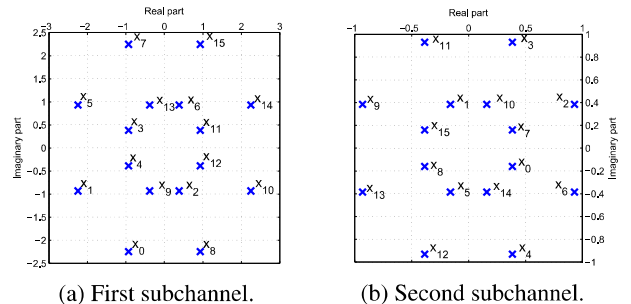
Table 1: The optimized binary representation in the constellation map of precoder $\max-d_{\min}$ for different mappings (each decimal value represents for 4 binary bits, *e.g.* $(8)_{10} = (1000)_2$).

Mapping	Mode	$[\mathbf{s}_0 \ldots \mathbf{s}_i \ldots \mathbf{s}_{15}]$
Gray-direct	$\mathbf{F}_{r_1/octa}$	[0 1 2 3 4 5 6 7 8 9 10 11 12 13 14 15]
Gray-like	$\mathbf{F}_{r_1}$	[0 1 2 3 9 8 11 10 6 7 4 5 15 14 13 12]
anti-Gray	$\mathbf{F}_{r_1}$	[14 5 1 10 8 3 7 12 15 4 0 11 13 2 6 9]
	$\mathbf{F}_{octa}$	[7 0 12 15 8 3 11 4 9 6 14 1 2 13 5 10]
MSEW	$\mathbf{F}_{r_1}$	[7 2 1 11 13 4 8 14 12 6 10 15 5 3 0 9]
	$\mathbf{F}_{octa}$	[2 5 7 0 9 12 10 15 11 14 8 13 4 3 1 6]

considered the Gray-like mapping for $\mathbf{F}_{r_1}$ only, in which we obtain $\bar{d}_\mathrm{H}(d_{min}) \simeq 1$. Regarding the constellation in Fig. 3, it is impractical to find the Gray-like mapping for $\mathbf{F}_{octa}$. On the other hand, $\bar{d}_\mathrm{H}(d_{min})$ is maximized for anti-Gray. We have $\bar{d}_\mathrm{H}(d_{min}) \simeq 3$ (case $\mathbf{F}_{r_1}$) and $\bar{d}_\mathrm{H}(d_{min}) = 2.5$ (case $\mathbf{F}_{octa}$) with anti-Gray mapping.

Given that $\mathbf{x}_i$ is equiprobable, if we define w_i the number of pairs of symbol vectors $\mathbf{s}_k$ and $\mathbf{s}_\ell$, such that $d_i = \|\mathbf{x}_k - \mathbf{x}_\ell\|$ for $\mathbf{x}_k \neq \mathbf{x}_\ell$, then the distribution of the distance d in the received constellation is given by $p(d = d_i) = w_i / \sum_j w_j$. Fig. 2b shows the distribution of all possible distances in the received constellation of $\mathbf{F}_{r_1}$. Let us denote the distances by $d_1 < \cdots < d_i < \cdots < d_{12}$. We define $\bar{S}(d_i)$ the averaged number of pairs of symbol vectors $\mathbf{s}_k$ and $\mathbf{s}_\ell$, such that $d_i = \|\mathbf{x}_k - \mathbf{x}_\ell\|$ and $d_H(\bar{\mathbf{s}}_k, \bar{\mathbf{s}}_\ell) = 1$. The values of $\bar{S}(d_i)$ are provided in Table 2 for $i \in \{1, 2, 3, 4\}$, considering $\mathbf{F}_d = \mathbf{F}_{\mathbf{r}_1}$ and the four mappings described in Table 1. Indeed, l_1 is maximum for MSEW ($l_1 = d_4$) compared to the other three for which $l_1 = d_1$. Due to space considerations, the distance distribution and $\bar{S}(d_i)$ are presented only for $\mathbf{F}_{r_1}$.

4. EXIT CHART ANALYSIS

We resort to the EXIT chart [11] to analyze the influence of the mapping strategy on the evolution of the MI between the *bit-interleaved coded* binary sequence $\bar{c}$ and its LLRs at in-

Table 2: Comparison of $\bar{S}(d_i)$, $i \in \{1, 2, 3, 4\}$ for $\mathbf{F}_{r_1}$.

	d_1	d_2	d_3	d_4
Gray-direct	2	0	0	2
Gray-like	3	0	0	0
anti-Gray	0.125	1	0.75	1.125
MSEW	0	0	0	1

put and output of the demapper. The *extrinsic* MI at output of demapper is a function of the *a priori* knowledge I_A^1 and the SNR. We define $I_E^1 = T_1\left(I_A^1, \text{SNR}\right)$. Similarly, $I_E^2 = T_2(I_A^2)$. The mathematical expressions of T_1 and T_2, which were deeply explained in [9, 11], are skipped in this paper due to space consideration. The mutual information is averaged over 100 trials. The signal-to-noise ratio is defined by $\text{SNR} = \frac{\sigma_s^2}{\sigma_\eta^2}\|\mathbf{H}\|_F^2 = \frac{\sigma_s^2}{\sigma_\eta^2}\rho^2$.
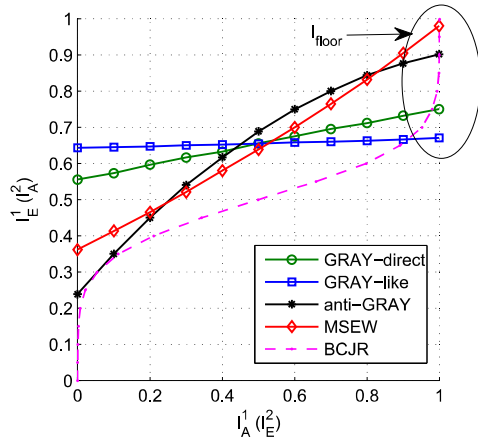
4.1. Error-floor analysis

Fig. 4: EXIT chart for the precoder $\mathbf{F}_{r_1}$ with $\gamma = 8.3^o$ and $\text{SNR} = 7.8$ dB; $\text{RSC}(13, 15)$.

Fig. 4 shows the EXIT chart in the case where $\text{SNR} = 7.8$ dB and channel angle $\gamma = 8.3^0$ (precoder $\mathbf{F}_{r_1}$), which was also used in [12]. The dashed line represents the EXIT function of the BCJR decoder of the $(13, 15)_{octal}$ RSC code, which is not dependent on SNR. The solid lines stand for the EXIT functions of the demapper for each mapping strategy. We obtain that, the traditional Gray-direct is not a good mapping since its ending point, which also accounts for the MI at error-floor region (I_{floor}), is lower than anti-Gray and MSEW, *i.e.* it achieves a poorer error-floor. The Gray-like mapping is even worse than Gray-direct and predicts no improvement in the iterative process. The best solution among those mappings is MSEW since its EXIT function shows the highest I_{floor}. The anti-Gray exhibits an acceptable I_{floor}. However, it gives the lowest starting point, which results in an early crossing at the turbo-cliff. Similar results are obtained for $\mathbf{F}_{octa}$.

Let us focus on the error-floor region to see the influence of the mapping in the selection modes of the precoder $\max-d_{\min}$ for different channel angles γ. We remind the switching threshold equal to $\gamma_0 = 17.28^o$. In Fig. 5, we have plotted the extrinsic information at the demapper output for both precoders and $I_A^1 = 1$. We obtain that the switching between $\mathbf{F}_{r_1}$ and $\mathbf{F}_{octa}$ has influence on the MI at the error floor for Gray-direct and anti-Gray mapping. Moreover the best γ threshold for concatenated scheme is $\gamma_0 \approx 30^o$. More importantly, we found that with the MSEW mapping, $\mathbf{F}_{r_1}$ always outperforms $\mathbf{F}_{octa}$. This makes the $\max-d_{\min}$ precoder more robust and simpler for the hardware design. This is a new-
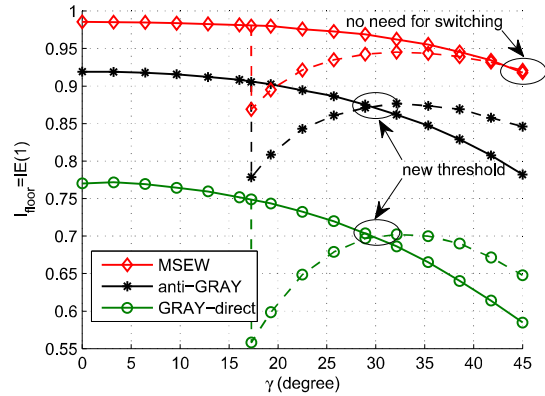

Fig. 5: The demapper *extrinsic* MI at the error floor with different channel angles γ at $\text{SNR} = 8.1$ dB.

found solution compared to the $\max-d_{\min}$ precoding scheme without FEC.
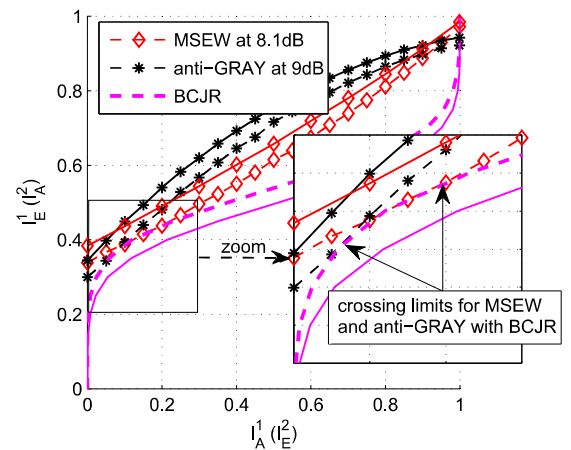
4.2. Turbo-cliff analysis

Fig. 6: EXIT chart with SNR_{lim} for turbo-cliff region.

In this subsection, we focus on the turbo-cliff region, where the EXIT functions of demapper and decoder form a bottleneck. The MSEW and anti-Gray mappings, which are more sensitive to the turbo-cliff region, are considered. Fig. 6 shows the EXIT charts and the SNR limitation (SNR_{lim}), where the two EXIT functions cross each other. In this figure, the average MI of I_E^1 and I_E^2 are presented in the solid lines, while the dashed lines represent the minimum MI over the 100 trials.

We can see that, with MSEW mapping, there is a possible intersection (between the EXIT functions measured by the minimum MI) at $\text{SNR} < \text{SNR}_{\text{lim}} = 8.1$ dB, while the SNR_{lim} of anti-Gray is 9 dB. Those values match perfectly with the turbo-cliff regions observed in error-rate performance plot, which will be presented in the next section.

5. SIMULATION RESULTS

The half-rate $(13, 15)_{octal}$-RSC code is used for the numerical evaluations. The frame length is 800 uncoded bits. The fixed channel with $\gamma = 8.3^o$ is considered. Let us denote by
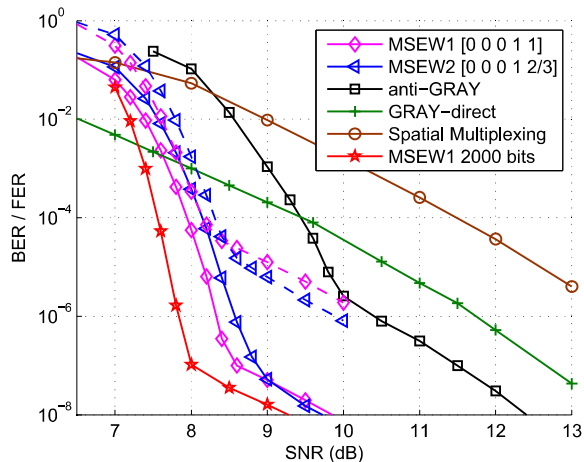
Fig. 7: BER (solid) and FER (dashed, only for MSEW) performance versus SNR of the mapping strategies.

MSEW-1 the MSEW mapping presented in Table 1 and Table 2. Fig. 7 shows the error-rate performance of the system with different mappings. The spatial multiplexing is also plotted as a reference for the case that CSI is unknown at the transmitter. We observe that the proposed MIMO symbol mapper associated with an optimized mapping rule significantly improves the performance. The MSEW-1 and anti-Gray respectively achieve a gain of 3.2 dB and 1.3 dB compared to the conventional Gray-direct at BER = 10^{-6}. Additionally, Fig. 7 also shows that the Gray-direct achieves a better BER performance compared to anti-Gray and MSEW at the SNR region that less than SNR$_{\text{lim}}$ as shown in Fig. 6.

The observed turbo-cliff is in accordance with the analysis done in Section 4. In terms of FER, the SNR limitation to overcome the bottleneck (and reach the error-floor) is equal to 8.1 dB for MSEW. It confirms the conclusions drawn from the EXIT chart. We also would like to point out that a better turbo-cliff can be achieved by varying $\bar{S}(d_i)$. Indeed, let us denote by MSEW-2 another MSEW solution, whose mapping for $\mathbf{F}_{r1}$ is [8 13 11 1 6 0 10 3 14 7 4 2 12 15 9 5]. This representation corresponds to Table-1. Thus, by varying $\bar{S}(d_5)$ (MSEW-2 has $\bar{S}(d_5) = 1$ and MSEW-1 has $\bar{S}(d_5) = \frac{2}{3}$), MSEW-2 achieves a better turbo-cliff compared to MSEW-1. However, it compensates for this advantage by a higher error-floor (see the FER in dashed lines). Note that the turbo-cliff can be further improved by increasing the frame length (see Fig.7, MSEW-1 2000 bits).

6. CONCLUSION

A MIMO symbol mapper is proposed in this paper to find the good mapping for the received constellation. Thanks to EXIT chart, we have shown that the mapping strategy of the symbol mapper has a great influence on the error-floor and the turbo-cliff regions. Moreover, depending on the mapping rule, the precoder $\max-d_{\min}$ can be used with a single mode ($\mathbf{F}_{r_1}$), which makes its design and practical application easier. Both simulated error-rate and EXIT chart analysis enable to draw the same conclusions. The MSEW symbol mapper is well adapted and significantly enhances the error-rate performance of the MIMO $\max-d_{\min}$ precoded system. As future work, in order to exploit the trade-off between the turbo-cliff and error-floor as observed from MSEW-1 and MSEW-2, it would be interesting to jointly optimize the two criteria *i.e.*, l_1 can be selected at a smaller distance, while $\bar{S}(l_1)$ and the others $\bar{S}(d_i)$ are further minimized.

Acknowledgment

REFERENCES

[1] Q. Li, G. Li, W. Lee, M. Lee, D. Mazzarese, B. Clerckx, and Z. Li, "MIMO techniques in WiMAX and LTE: a feature overview," *IEEE Commun. Mag.*, vol. 48, no. 5, pp. 86–92, 2010.

[2] A. J. Paulraj, D. A. Gore, R. U. Nabar, and H. Bolcskei, "An overview of MIMO communications-a key to gigabit wireless," *Proc. of the IEEE*, vol. 92, no. 2, pp. 198–218, 2004.

[3] L. Collin, O. Berder, P. Rostaing, and G. Burel, "Optimal minimum distance-based precoder for mimo spatial multiplexing systems," *IEEE Trans. on Signal Processing*, vol. 52, no. 3, pp. 617–627, 2004.

[4] P. Rostaing, O. Berder, G. Burel, and L. Collin, "Minimum BER diagonal precoder for MIMO digital transmissions," *Signal Processing*, vol. 82, no. 10, pp. 1477–1480, 2002.

[5] E. Telatar, "Capacity of multi-antenna gaussian channels," *Eur. Trans. Telecom.*, vol. 10, no. 6, pp. 585–595, 1999.

[6] A. Picart, P. Didier, and A. Glavieux, "Turbo-detection: a new approach to combat channel frequency selectivity," in *IEEE Int. Conf. on Commun. Towards the Knowledge Millennium*, 1997, vol. 3, pp. 1498–1502.

[7] S. Haykin, M. Sellathurai, Y. de Jong, and T. Willink, "Turbo-mimo for wireless communications," *IEEE Commun. Mag.*, vol. 42, no. 10, pp. 48–53, 2004.

[8] L.R. Bahl, J. Cocke, F. Jelinek, and J. Raviv, "Optimal decoding of linear codes for minimizing symbol error rate," *IEEE Trans. on Info. Theory*, pp. 284–287, Mar. 1974.

[9] S. Ten-Brink, "Designing iterative decoding schemes with the extrinsic information transfer chart," *AEU Int. J. Electron. Commun.*, vol. 54, no. 6, pp. 389–398, 2000.

[10] J. Tan and G. L. Stuber, "Analysis and design of symbol mappers for iteratively decoded bicm," *IEEE Trans. on Wireless Commun.*, vol. 4, no. 2, pp. 662–672, 2005.

[11] J. Hagenauer, "The exit chart-introduction to extrinsic information transfer in iterative processing," in *Proc. 12th EUSIPCO*, 2004, pp. 1541–1548.

[12] C. Xiao, Y. R. Zheng, and Z. Ding, "Globally optimal linear precoders for finite alphabet signals over complex vector gaussian channels," *IEEE Trans. on Signal Processing*, vol. 59, no. 7, pp. 3301–3314, 2011.